A fully implicit finite volume scheme for single phase flow with reactive transport in porous media

Etienne Ahusborde, Brahim Amaziane, Mustapha El Ossmani

Version of Record: https://www.sciencedirect.com/science/article/pii/S0378475418302118
Manuscript_e4aa3d2a6ba4dc10f6cdc0376c2e01bd

A fully implicit finite volume scheme for single phase flow with reactive transport in porous media

E. Ahusborde [a,*], M. El Ossmani[a,b], M. Id Moulay[a]

[a] *CNRS / Univ Pau & Pays Adour / E2S UPPA, Laboratoire de Mathématiques et de leurs Applications de Pau, Fédération IPRA, UMR5142, 64000, Pau, France.*
[b] *University Moulay Ismail, EMMACS-ENSAM, Marjane II, 50000 Meknès, Morocco.*

Abstract

Single phase flow and reactive transport modelling involve solving a highly nonlinear coupled system of partial differential equations to algebraic or ordinary differential equations requiring special numerical treatment. In this paper, we propose a fully implicit finite volume method using a direct substitution approach to improve the efficiency and the accuracy of numerical computations for such systems. The approach has been developed and implemented in the framework of the parallel open-source platform DuMu^X. The object oriented code allows solving reactive transport problems considering different coupling approaches. A number of 2D and 3D numerical tests were performed for verifying and demonstrating the capability of the coupled fully implicit approach for single phase flow and reactive transport in porous media. Numerical results for the reactive transport benchmark of MoMaS and long-term fate of injected CO_2 for geological storage including a comparison between the direct substitution approach and the sequential iterative approach are presented. Parallel scalability is investigated for simulations with different grid resolutions.

Keywords: Single phase multicomponent flow, Reactive transport, Porous media, Fully implicit approach, DuMu^X, Parallel algorithm.

*Corresponding author
Email address: etienne.ahusborde@univ-pau.fr (E. Ahusborde)

1. Introduction

Reactive transport modelling in porous media plays a significant role for many subsurface applications in geological and reservoir engineering processes as for instance the sequestration of CO_2 in saline aquifers, the geological storage of nuclear waste or the prevention of groundwater pollution and the contaminant remediation.

Carbon Capture and Storage (CCS) is a promising way to mitigate the effects of global warming. Assessing the viability of geological storage must rely on numerical simulations due to the long time scales involved. Several physical and geochemical trapping mechanisms must be combined to ensure a high containment rate, and geochemical trapping becomes increasingly important over longer time scales [30]. Carbon dissolution in water occurs over hundreds of years, and formation of carbonate minerals over millions of years, see [19]. Many references can be found for the numerical approximation of such phenomena, see for instance [9, 42]. The main issue concerning the geological storage of CO_2 is the simulation of the different trapping mechanisms. In [41], the authors show that modified single phase flow models can predict pressure build-up far from the injection as well as complex two-phase flow model. Single phase flow is considered for instance in [25] and [35]. In [25], in the framework of SHPCO2 Project, the gas phase is assumed to be immobile and therefore gaseous carbon dioxide is considered as a fixed species neglecting the two-phase flow effects. In [35], an initial amount of supercritical CO_2 is converted into a source term of liquid CO_2 and then the authors study the transport of the dissolved CO_2 and the precipitation/dissolution process of minerals. In [4], the authors employ a one-phase reactive flow to model the leaking of CO_2-saturated brine in a fractured pathway once supercritical CO_2 is totally dissolved. CO_2 is generally injected in its supercritical form. This injection may induce important pressure build-up that can damage the reservoir or induce fracturing and seismic events. Moreover, the supercritical CO_2 that is less dense than the brine present in the aquifer, will migrate vertically firstly and then along the top of the aquifer. Finally it builds up under the cover rock inducing a risk of leakage through faults. In [43], the authors propose an alternative strategy that consists in injecting dissolved CO_2 to circumvent the above-mentioned risks and increase the security of its geological sequestration. In [5], a study of this process and its interactions with the carbonate reservoir through geochemical reactions is proposed.

Single phase multicomponent reactive flows are modelled by a mass bal-

ance law, Darcy's law and equations of state. Coupling between flow and chemistry occurs through reactions rates. In the case of equilibrium reactions, these rates are unknowns and are commonly eliminated through linear transformations [37, 39] and replaced by mass actions laws that are algebraic equations relating the activities of concerned species. For kinetic reactions, the rates are nonlinear functions of concentrations [14] and involve ordinary differential equations. By consequence, the problem is modelled by a system of partial differential equations (describing a compositional flow) coupled with algebraic or ordinary differential equations related to chemical reactions. The numerical strategies for solving this system can be divided into three dominant algorithms: the global implicit (GIA), the sequential iterative (SIA) and sequential non-iterative (SNIA) approaches [44, 46]. In the GIA, the nonlinear system gathering all equations is solved at each time step. For the sequential solution approaches, flow and reactive transport (or possibly, flow, transport and chemistry) are solved sequentially at each time step. The difference between the SIA and SNIA lies on the fact that for the SIA, the procedure is present in an iterative loop. Sequential approaches are also named operator-splitting approaches.
In comparison with GIA, sequential approaches can be easier to implement since existing codes and specific methods can be used for each subproblem (flow, transport, chemistry). Nonetheless, sequential approaches introduce operator splitting errors [11, 45] and restrictions on the time step are mandatory to ensure mass conservation for instance. In [46], the authors describe the GIA as "research tools for one-dimensional investigations" due to their complexity and their high computational requirements. Thanks to the advance of high-performance computing in the last decades, these restrictions are no longer relevant. The Groupement Mathematical Modelling and Numerical Simulation for Nuclear Waste Management has proposed in [18] a benchmark to test numerical methods used to deal with reactive transport problem in porous media. In this framework several sequential and implicit algorithms have been compared. In [16] and [34], the authors propose respectively a SIA and a SNIA. The other participants [10, 20, 28, 38] deal with various global implicit algorithms. More precisely, in [10], the authors propose a method where the chemical problem is eliminated locally, leading to a nonlinear system where the transport and chemistry subsystems remain separated. In [20, 21], the problem is written in the form of differential algebraic equations (DAE). In [28], the author use a reduction technique introduced in [32, 33] that aims to reduce the number of coupled nonlinear differential

equations drastically. Finally in [38], a direct substitution approach (DSA) consisting in substituting the equations of chemistry directly in the equations of transport is employed. In [17], the results provided by the different teams are compared with a good agreement. The different benchmarks showed that sequential approaches can be as accurate as global ones provided they are carefully implemented while global approaches are now more efficient that was originally believed.

This work aims to develop a GIA to perform numerical simulation of single phase multicomponent flows with reactive transport in porous media. In [7, 8], in the context of two-phase flow, we proposed a sequential approach that splits the original problem into two sub-problems. The first sub-problem computes an implicit two-phase compositional flow where only species present in both phases are taken into account. The second sub-problem calculates a reactive transport problem where flow properties (Darcy velocity for each phase, saturation of each phase, temperature, density,...) are given by the first step. A SIA has been implemented for the reactive transport sub-problem. To improve the robustness of the scheme and the accuracy loss due to the time-splitting involved by the SIA, in [6], we switched to a GIA for reactive transport subsystem. More precisely, we used a DSA [46]. The goal of this paper is to focus on the single phase flow reactive problem to validate our implementation of the DSA and to compare the DSA and the SIA to emphasize the improvements made by the implicit approach. It is worth noting that here, the comparison between the DSA and SIA is done in the same numerical environment. Examination of the existing literature sees a clear trend in evaluating the efficiency of the different methods through calculations performed on different codes or computer facilities.

The rest of the paper is organized as follows. In section 2, we describe the governing equations for a single phase multicomponent flow with reactive transport and the global implicit approach. In section 3, the finite-volume discretization of the problem is detailed and some reminders about the SIA are given. In section 4, a description of the implementation of our strategy in the free and open-source simulator DuMu^X [1, 24] is given and some numerical results for the benchmark MoMaS and for examples dealing with geological sequestration of CO_2 are proposed. On a particular example of the SHPCO2 Project [25], an advanced comparison between the DSA and the SIA is given in term of computational time for several grid resolutions. Some three-dimensional parallel computations are presented with good strong and weak parallel efficiencies.

2. Formulation of the problem

In this section, we describe the geochemical model and the mathematical model for single phase multicomponent flow with reactive transport in porous media. Finally, we present the formulation of GIA that will be used in the sequel.

2.1. Geochemical model

We note by I the set of all the N_c chemical components involved in N_r chemical reactions. Chemical reactions can be classified in two categories. By convention, equilibrium reactions are assumed to be sufficiently fast and reversible while kinetic reactions are slow or irreversible, the notion of velocity and reversibility being system and scale dependent. We assume that the N_r reactions are decomposed into N_e equilibrium reactions and N_k kinetic reactions. Following the Morel formalism [40], we split the set of all chemical species I into N_p primary and N_s secondary species noted respectively I_p and I_s ($I = I_p \cup I_s$). If we assume that the stoichiometric matrix has full rank (there are no redundant reactions), each chemical reaction can be expressed as the formation of a single secondary species from the set of primary species:

$$A_j = \sum_{i \in I_p} \nu_{ji} A_i, \ j \in I_s,$$

where ν_{ji} is the stoichiometric coefficient of the species A_i in the reaction j.

Following the convention established in [18], the set of primary components I_p is decomposed into mobile primary components I_{pm} and immobile primary components I_{pi} ($I_p = I_{pm} \cup I_{pi}$). The set of secondary components I_s is split into mobile secondary components I_{sm}, immobile secondary components I_{si} and components involved in kinetic reactions I_{sk} ($I_s = I_{sm} \cup I_{si} \cup I_{sk}$). $N_q = \text{card}\{I_{sm} \cup I_{si}\}$ is the number of reactions at equilibrium and $N_k = \text{card}\{I_{sk}\}$ is the number of kinetic reactions such that $N_q + N_k = N_r$.

2.1.1. Chemical equilibrium

Each equilibrium reaction gives rise to an algebraic relation called mass action law that links the activities of the species involved in the reaction. The mass action law writes as follows:

$$a^j = K_j \prod_{i \in I_p} (a^i)^{\nu_{ji}}, \ j \in I_{sm} \cup I_{si}, \tag{1}$$

where a^j is the activity of species j, K_j is the equilibrium constant of reaction j.

2.1.2. Kinetics

Mass action laws apply only for equilibrium reactions. Otherwise, slow chemical reactions are characterized by a reaction rate r_j depending, among others, on the activities of the species present in the reaction. In this work, we consider only kinetic reaction describing precipitation/dissolution of a mineral. For the expression of the kinetic rate, we use the form given in [22], simplified from that introduced in [14]. Each kinetic reaction leads to an ordinary differential equation:

$$\frac{dc^j}{dt} = -r_j, \text{ with } r_j = K_j^s A_j^s \left(1 - K_j \prod_{i \in I_p} (a^i)^{\nu_{ji}}\right), \ j \in I_{sk}, \tag{2}$$

where c^j denotes the concentration of the kinetic species j while K_j^s and A_j^s are respectively the kinetic-rate constant [mol.m^{-2}.s^{-1}] and the reactive surface [m^2.m^{-3}] of component j.
When mineral c^j supersaturated, $K_j \prod_{i \in I_p} (a^i)^{\nu_{ji}} > 1$ and the mineral precipitates. When the mineral is undersaturated, it dissolves because $K_j \prod_{i \in I_p} (a^i)^{\nu_{ji}} < 1$.

2.2. Mathematical model for single phase multicomponent flow with reactive transport

We consider the mass balance equation (see for instance [26]) for primary and secondary species:

$$\frac{\partial}{\partial t}(\phi c^i) + \nabla \cdot (c^i \vec{q}) - \nabla \cdot (D \nabla c^i) = \sum_{j \in I_s} \nu_{ji} r_j, \ i \in I_{pm}, \tag{3}$$

$$\frac{d}{dt}(c^i) = \sum_{j \in I_s} \nu_{ji} r_j, \ i \in I_{pi}, \tag{4}$$

$$\frac{\partial}{\partial t}(\phi c^i) + \nabla \cdot (c^i \vec{q}) - \nabla \cdot (D \nabla c^i) = -r_i, \ i \in I_{sm}, \tag{5}$$

$$\frac{d}{dt}(c^i) = -r_i, \ i \in I_{si} \cup I_{sk}, \tag{6}$$

where ϕ [-] denotes the porosity of the medium, c^i is the molar concentration of species i [mol.m^{-3}], D [m^2.s^{-1}] denotes the diffusion-dispersion tensor:

$$D = \phi \left(D_m \mathbb{I} + d_L |\vec{q}| \mathbb{I} + (d_L - d_T) \frac{\vec{q}\vec{q}^T}{|\vec{q}|} \right).$$

D_m [m^2.s^{-1}] is the molecular diffusion, d_L [m] and d_T [m] are the magnitudes of longitudinal and transverse dispersion respectively and $\vec{q}$ [m.s^{-1}] is the Darcy velocity, expressed as follows:

$$\vec{q} = -\frac{\mathbb{K}}{\mu}(\nabla P - \rho \vec{g}), \tag{7}$$

where μ [Pa.s] is the dynamic viscosity, $\mathbb{K}$ [m^2] is the absolute permeability tensor, P [Pa] is the pressure, ρ [kg.m^{-3}] is the mass density and $\vec{g}$ [m.s^{-2}] is the gravitational acceleration. Finally, r_j [mol.m^{-3}.s^{-1}] is the rate of reaction j (it can be equilibrium if $j \in I_{sm} \cup I_{si}$ or kinetic if $j \in I_{sk}$).
For the sake of simplicity, we introduce the advection-diffusion operator:

$$L(c) = \nabla \cdot (c\vec{q}) - \nabla \cdot (D \nabla c). \tag{8}$$

In order to eliminate the reaction rates r_j in equations (3)-(4), we make linear combinations between equations (5)-(6) with each equation (3)-(4). This introduces N_p new conservation laws that write:

$$\frac{\partial}{\partial t} \left(\phi c^i + \sum_{j \in I_{sm}} \phi \nu_{ji} c^j + \sum_{j \in I_{si} \cup I_{sk}} \nu_{ji} c^j \right) + L(c^i + \sum_{j \in I_{sm}} \nu_{ji} c^j) = 0, \ i \in I_{pm}, \tag{9}$$

$$\frac{d}{dt} \left(c^i + \sum_{j \in I_{si} \cup I_{sk}} \nu_{ji} c^j \right) = 0, \ i \in I_{pi}. \tag{10}$$

To retrieve the same number of equations as there are unknowns, the N_s equations (5)-(6) are replaced by N_e mass actions laws defined by (1) corresponding to the equilibrium reactions and N_k ordinary differential equations corresponding to the kinetic reactions given by (2).

Remark. *The equilibrium reaction rates are eliminated because they are unknown while kinetic rates are known (see for instance equation (2)). In this work, all the reaction rates are eliminated, including kinetic reaction*

rates. This is why, there is no reaction rate in the right hand side of equations (9)-(10). In the left hand side of these equations, the concentration of the secondary kinetics species (c^j, $j \in I_{sk}$) are part of the unknowns. These concentrations are governed by the ordinary differential equations (2). Another strategy would consist in eliminating only the equilibrium reactions rate in equations (9)-(10) and in incorporating the kinetic reaction rates directly into the right hand side of these latter equations as a source/sink term.

2.3. Formulation of the global implicit approach

In [7, 8], we adopted a SIA to solve the reactive transport problem. In the present work, we consider a GIA, where a DSA is adopted. The system of equations describing the reactive transport problem writes:

$$\frac{\partial}{\partial t}\left(\phi c^i + \sum_{j\in I_{sm}} \phi \nu_{ji} c^j + \sum_{j\in I_{si}\cup I_{sk}} \nu_{ji} c^j\right) + L(c^i + \sum_{j\in I_{sm}} \nu_{ji} c^j) = 0, \quad i \in I_{pm}, \tag{11}$$

$$\frac{\partial}{\partial t}\left(c^i + \sum_{jT\in I_{si}\cup I_{sk}} \nu_{ji} c^j\right) = 0, \quad i \in I_{pi}, \tag{12}$$

$$a^j = K_j \prod_{i\in I_p} (a^i)^{\nu_{ji}}, \quad j \in I_{sm} \cup I_{si}, \tag{13}$$

$$\frac{dc^j}{dt} = -K_j^s A_j^s \left(1 - K_j \prod_{i\in I_p} (a^i)^{\nu_{ji}}\right), \quad j \in I_{sk}. \tag{14}$$

The DSA consists in incorporating equations (13)-(14) in mass balance equations (11)-(12).

3. Numerical scheme

In this section, we describe the fully implicit finite volume scheme used for the discretization of the problem (11)-(14). In the sequel, the GIA will be compared with the SIA implemented in [7, 8]. Consequently, for the sake of clarity, the SIA is also described.

3.1. Finite volume discretization of single phase multicomponent flow with reactive transport

The spatial discretization of the coupled system (11)-(14) employs a conservative Finite Volume (FV) method based on a fully upwinding scheme to treat the convective terms and a conforming finite element scheme with piecewise linear elements for the diffusive terms. The time discretization is done by an implicit Euler method.

Here, we choose a fully implicit cell-centred FV method. It consists in integrating the equations (11)-(14) on a control volume V_k (see Figure (1)) and evaluating the fluxes at the interface γ_{kl} between two adjacent elements V_k and V_l.

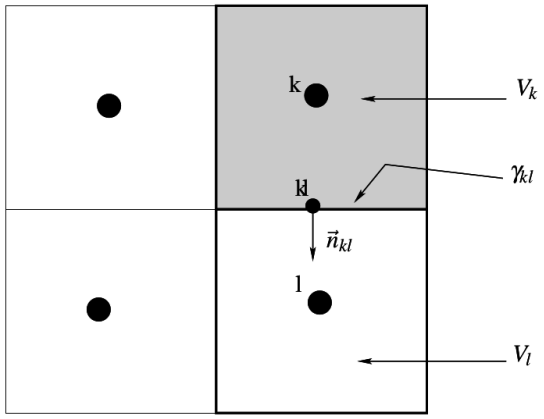

Figure 1: Discretization by the cell centred finite volume method.

By using the implicit Euler scheme for the time discretization and due to the fact that the primary unknowns (P, c^i) and the physical parameters are constant on each element V_k, the cell-centred FV scheme corresponding to system (11)-(14) is given by:

$$\frac{|V_k|}{\Delta t^n}\left(\left\{\phi c^i+\sum_{j\in I_{sm}}\nu_{ji}\phi c^j+\sum_{j\in I_{si}\cup I_{sk}}\nu_{ji}c^j\right\}_k^{n+1}\right.$$
$$\left.-\left\{\phi c^i+\sum_{j\in I_{sm}}\nu_{ji}\phi c^j+\sum_{j\in I_{si}\cup I_{sk}}\nu_{ji}c^j\right\}_k^{n}\right)$$
$$+\sum_{l\in V(k)}|\gamma_{kl}|\left(\left\{c^i\right\}_{kl}^{n+1}\left\{\vec{q}\right\}_{kl}^{n+1}+\sum_{j\in I_{sm}}\nu_{ji}\left\{c^j\right\}_{kl}^{n+1}\left\{\vec{q}\right\}_{kl}^{n+1}\right)\cdot\vec{n}_{kl}$$
$$-\sum_{l\in V(k)}|\gamma_{kl}|\left(\left\{D\right\}_{kl}^{n+1}\left\{\nabla c^i\right\}_{kl}^{n+1}+\sum_{j\in I_{sm}}\nu_{ji}\left\{D\right\}_{kl}^{n+1}\left\{\nabla c^j\right\}_{kl}^{n+1}\right)\cdot\vec{n}_{kl}$$
$$=0,\ i\in I_{pm}, \tag{15}$$

$$\frac{|V_k|}{\Delta t^n}\left(\left\{c^i+\sum_{j\in I_{si}\cup I_{sk}}\nu_{ji}c^j\right\}_k^{n+1}-\left\{c^i+\sum_{j\in I_{si}\cup I_{sk}}\nu_{ji}c^j\right\}_k^{n}\right)=0,\ i\in I_{pi}, \tag{16}$$

$$\left\{a^j\right\}_k^{n+1}=K_j\prod_{i\in I_p}\left\{(a^i)^{\nu_{ji}}\right\}_k^{n+1},\ j\in I_{sm}\cup I_{si}, \tag{17}$$

$$\left\{c^j\right\}_k^{n+1}=\left\{c^j\right\}_k^{n}-\Delta t^n\ K_j^sA_j^s\Big(1-K_j\prod_{i\in I_p}\left\{(a^i)^{\nu_{ji}}\right\}_k^{n+1}\Big),\ j\in I_{sk}, \tag{18}$$

$$\left\{\vec{q}\right\}_{kl}^{n+1}=-\left\{\frac{\mathbb{K}}{\mu}\right\}_{kl}\left(\left\{\nabla P\right\}_{kl}^{n+1}-\left\{\rho\right\}_{kl}^{n+1}\vec{g}\right), \tag{19}$$

where $\vec{n}_{kl}$ denotes the unit outer normal to γ_{kl}, $V(k)$ is the set of adjacent elements of V_k.

Now to define the finite volume scheme it is enough to approach the convective and the diffusive fluxes on the interfaces γ_{kl}. For this purpose, a fully upwinding scheme is used to calculate the numerical flux for the convective term. More precisely, the quantities $(P,\ c^i)$ are evaluated implicitly and upstream at the interface γ_{kl} between two adjacent elements as:

$$\{\cdot\}_{kl}^{n+1}=\begin{cases}\{\cdot\}_k^{n+1} & \text{if}\quad \{\vec{q}\}_{kl}^{n+1}\cdot\vec{n}_{kl}>0\\ \{\cdot\}_l^{n+1} & \text{else}\ .\end{cases} \tag{20}$$

The gradient operators on the interfaces γ_{kl} are calculated by a $\mathbb{P}_1/\mathbb{Q}_1$ finite element method with piecewise linear elements. An harmonic average of the values between two adjacent elements is used to calculated the absolute permeability $\{\mathbb{K}\}_{kl}$ that is considered as a scalar and the diffusion coefficients $\{D\}_{kl}^{n+1}$ at the interface γ_{kl}. $\{\rho\}_{kl}^{n+1}$ is computed as the arithmetic average of two elements V_k and V_l.

3.2. Sequential iterative approach

We give here some reminders about the SIA used in [7, 8] where problem (11)-(14) is expressed as follows:

$$\begin{aligned} \phi\frac{\partial T_m}{\partial t} + \frac{\partial T_f}{\partial t} + L(T_m) &= 0, && (21)\\ T &= T_m + T_f, && (22)\\ T_f &= \Psi_C(T), && (23) \end{aligned}$$

with

$$T_m^i = \begin{cases} c^i + \displaystyle\sum_{j\in I_{sm}} \nu_{ji} c^j, \ i \in I_{pm}, \\ 0, \ i \in I_{pi}, \end{cases} \quad \text{and} \quad T_f^i = \begin{cases} \displaystyle\sum_{j\in I_{si}\cup I_{sk}} \nu_{ji} c^j, \ i \in I_{pm}, \\ c^i + \displaystyle\sum_{j\in I_{si}\cup I_{sk}} \nu_{ji} c^j, \ i \in I_{pi}. \end{cases} \tag{24}$$

T_m is the vector of the total mobile concentrations for each primary species and T_f is the vector of the total immobile concentrations.
With this formulation, the SIA states as follows: supposing $T_m^n, T_m^{n+1,k}, T_f^n, T_f^{n+1,k}$ are known, $T^{n+1,k+1}, T_m^{n+1,k+1}, T_f^{n+1,k+1}$ are computed thanks to the following iterative scheme:

$$\begin{aligned} \phi\frac{T_m^{n+1,k+1} - T_m^n}{\Delta t} + \frac{T_f^{n+1,k} - T_f^n}{\Delta t} + L(T_m^{n+1,k+1}) &= 0, && (25)\\ T^{n+1,k+1} &= T_m^{n+1,k+1} + T_f^{n+1,k}, && (26)\\ T_f^{n+1,k+1} &= \Psi_C(T^{n+1,k+1}), && (27) \end{aligned}$$

where $T_m^{n,k}$ denotes the approximation of quantity T_m at time t^n and at iteration k in the iterative loop of the SIA algorithm.

The iterative algorithm is stopped when a given tolerance $\epsilon_{SIA} \ll 1$ is reached:

$$\frac{||T_m^{n+1,k+1} - T_m^{n+1,k}||}{||T_m^{n+1,k+1}||} + \frac{||T_f^{n+1,k+1} - T_f^{n+1,k}||}{||T_f^{n+1,k+1}||} < \epsilon_{SIA},$$

where $||.||$ is a discrete L^2 norm.

Equation (27) corresponds to the resolution of a nonlinear problem related to the chemical equilibrium wherein the discretized ordinary differential equations involved in kinetic reactions have been introduced. This resolution aims at computing the concentrations of the primary components from the total concentrations $T^{n+1,k+1}$ to update the total immobile concentrations $T_f^{n+1,k+1}$ and pursue the iterative algorithm. The nonlinear system is composed of N_p equations related to the total concentration of each primary component in which the mass actions laws have been introduced plus N_k discretized ordinary differential equations (one for each kinetic reaction). It is solved by the multidimensional root-finding functions of GSL [3]. The unknowns are the concentrations of the primary components and the concentrations of the secondary kinetic species.

4. Numerical simulations

All our developments have been implemented in DuMu^X [1, 24], a free and open-source simulator for flow and transport processes in porous media, based on the Distributed and Unified Numerics Environment DUNE [2]. In this section, we describe this implementation and we present several test cases to validate our approach.

4.1. Development and implementation of our strategy

In [7], we had developed in the DuMu^X framework a single phase multicomponent transport module named $1pmc - react$. In this context, we had implemented a new $1pmc$ module (one-phase, m-component) that was coupled with the calculations of the chemical problem computed with GSL [3] through a SIA described in subsection 3.2.
Here, we propose to replace the SIA by a GIA. More precisely, we use a DSA that consists in integrating directly the mass action laws (17) in the discretized conservation laws (15)-(16). So we have modified the module

$1pmc - react$ by introducing the mass actions laws in the balance equations. The approach is fully implicit. The spatial discretization is performed by the cell-centred finite volume approach described in subsection (3.1) by equations (15)-(19).

The nonlinear system is solved by a Newton method and a preconditioned BiConjugate Gradient STABilized (BiCGSTAB) method is used to solve the linear system. Numerical differentiations techniques are used to approximate the derivatives in the calculation of the Jacobian matrix. The control of the time-step is based on the number of iterations required by the Newton method to achieve convergence for the last time iteration. The time-step is reduced, if the number of iterations exceeds a specified threshold, whereas it is increased if the method converges within less iterations.

4.2. Numerical results

To validate our strategy, several tests have been performed. Here, we focus on three tests cases. The first one is the reactive transport benchmark of MoMaS [18] and its goal is to validate the implementation of the GIA. The second and third test cases deal with examples of geological sequestration of CO_2. More precisely, the second test case proposed in [15, 31] focus on the interactions of CO_2 with minerals by considering only equilibrium reactions. Finally, the last test case is a scenario of geological sequestration of CO_2 in saline aquifers and was proposed in the framework of SHPCO2 Project [25]. We propose to compare the GIA and SIA developed in [7] for this example. The comparison focuses on the computational time and more precisely, on the management of the time-step for both strategies during the simulations. Three dimensional parallel computations have been performed. Good strong and weak efficiencies are obtained.

4.2.1. Reactive transport benchmark of MoMaS

The Groupement MoMaS has proposed in [18] a benchmark to test numerical methods used to deal with reactive transport problem in porous media. This benchmark is composed of three test cases with increasing difficulties named “Easy test case”, “Medium test case” and “Hard test case”. For each case, two values of the diffusivity coefficients are proposed to test the codes both under advective and diffusive transport conditions. The definition of the benchmark is not repeated here since its detailed description can be found in [18]. We have performed the three cases but we present in the sequel only

results for the 1D and 2D "Advective easy test case" and the 2D "Diffusive hard test case".

Easy test case. The easy test case consists of four mobile and one immobile primary components involved in seven reactions. Only equilibrium reactions are considered. This test aims to validate our implementation of the DSA in the DuMu^X framework.

For the easy 1D advective test case, Figure 2 displays the concentration profile of the fixed component S at $t = 10\ s$ near the inlet of the domain for several grid resolutions. This profile is characterized by sharp concentration fronts with a peak due to the disequilibrium induced by the injection of species X_3. The location and the peak amplitude are close to those computed by all the participants in [17]. Nonetheless, we can observe that our results are closest to those obtained in [38] where a DSA was also considered. Figure 3 represents the magnitude of time step as a function of the time simulation for the 1D easy advective test case with a non-uniform grid composed of 240 elements (refined in the medium B that is more reactive as suggested by several participants of the benchmark). A maximum time step equal to 10 s was enforced. A similar behaviour of the time step evolution can be observed in [38]. It proves that in this example, DSA can use large time steps.

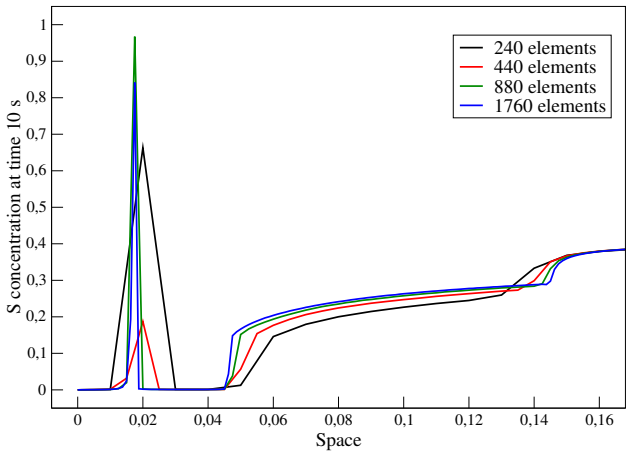

Figure 2: Local concentration profiles of solid component S at time 10 for the 1D easy advective test case (subregion: $x = 0$ to $x = 0.16$) for different grid resolutions

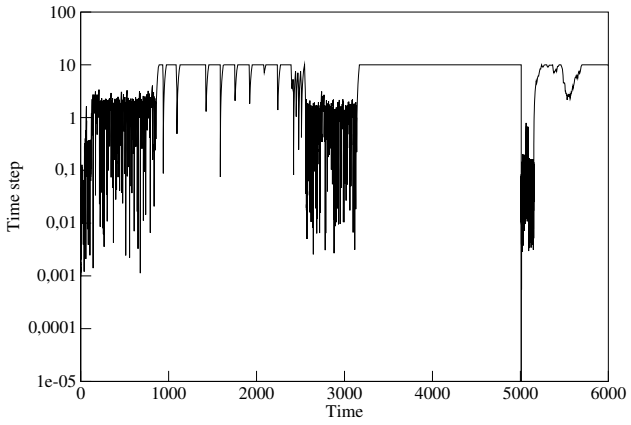

Figure 3: Magnitude of time step versus time simulation for the 1D easy advective test case with a non-uniform grid of 240 elements (a maximum time step equal to 10 s is enforced).

For the 2D advective easy test case, Figure 4 represents the concentrations for the primary components X_1, X_2, X_3 and S at $t = 1000\ s$ on a mesh composed of 210×100 elements. These results are close to those obtained in [27] where the concentrations of all the components are depicted and those in [17, 29] where only concentration of X_3 is discussed. An initial time step equal to $10^{-15}\ s$ and a maximal time step equal to $0.1\ s$ have been used.

Hard test case. In comparison with the easy test case, the additional difficulty is the presence of two equilibrium precipitation/dissolution reactions and one kinetic reaction. In total, there are twelve reactions. For each precipitated species P_i, a solubility product must be respected:

$$\text{if } K_{P_i} \prod_{j=1}^{N_{pm}} (c^j)^{\nu_{ij}} < 1 \text{ then } c_{P_i} = 0 \text{ else } K_{P_i} \prod_{j=1}^{N_{pm}} (c^j)^{\nu_{ij}} = 1. \tag{28}$$

K_{P_i} is a reaction constant, N_{pm} is the number of primary mobile components, ν_{ij} are stoichiometric coefficients. c^j represents the concentration of the primary mobile components and c_{P_i} denotes the concentration of the precipitated/dissolved species P_i. This complementary problem is reformulated as:

$$\min \left(c_{P_i}, 1 - K_{P_i} \prod_{j=1}^{N_{pm}} (c^j)^{\nu_{ij}} \right) = 0, \tag{29}$$

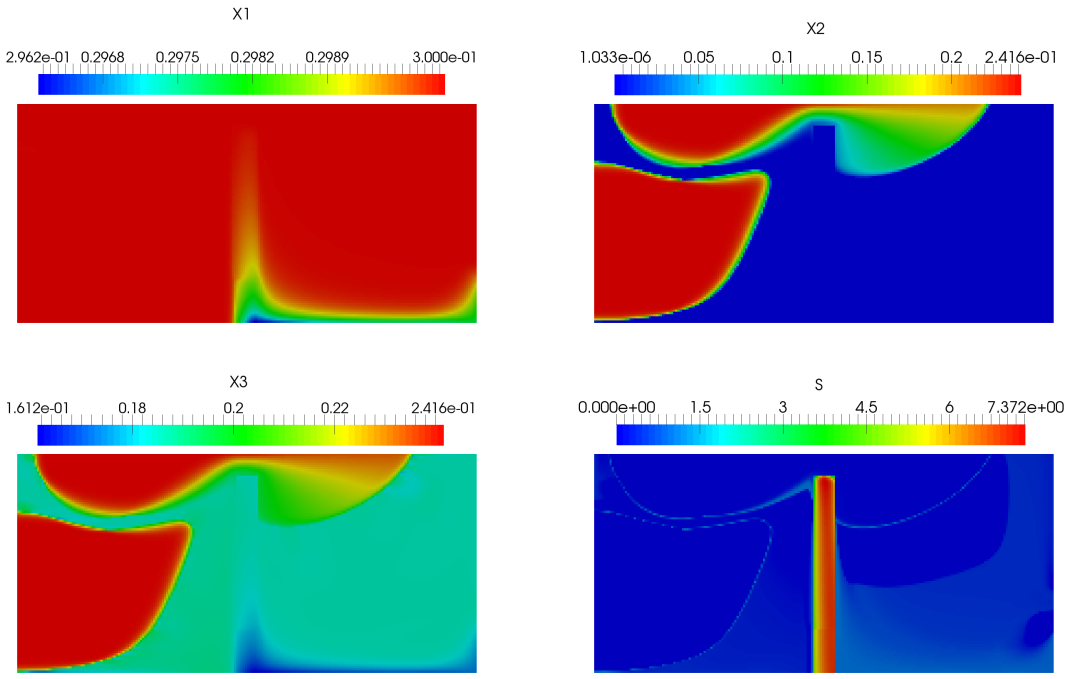

Figure 4: Concentrations of components X_1, X_2, X_3 and S at $t = 1000\ s$ for the 2D advective easy test case.

or using for instance the Fischer-Burmeister complementary function [23]:

$$\sqrt{{c_{P_i}}^2 + \left(1 - K_{P_i} \prod_{j=1}^{N_{pm}} (c^j)^{\nu_{ij}}\right)^2} - c_{P_i} - \left(1 - K_{P_i} \prod_{j=1}^{N_{pm}} (c^j)^{\nu_{ij}}\right) = 0. \qquad (30)$$

Remark. *In this work, we consider the min function. In the DuMu^X framework, nonlinear complementarity functions are already used to solve transition conditions formulated firstly as a set of local inequality constraints for miscible multiphase flow in porous media [36]. In the Newton method, the Jacobian matrix is computed by numerical differentiation.*
Equation $\min\left(c_{P_i}, 1 - K_{P_i} \prod_{j=1}^{N_{pm}} (c^j)^{\nu_{ij}}\right) = 0$ *that is piecewise differentiable is considered as a supplementary equation. During the Newton iterative algorithm, the minimum of the quantities* c_{P_i} *and* $1 - K_{P_i} \prod_{j=1}^{N_{pm}} (c^j)^{\nu_{ij}}$ *is com-*

puted and then, either the equation $c_{P_i} = 0$ is considered, or it is the equation $1 - K_{P_i} \prod_{j=1}^{N_{pm}} (c^j)^{\nu_{ij}} = 0$.

Figure 5 depicts the concentration of component P_1 for the 2D advective hard test case. A very similar picture can be found in Figure 7 of [38]. As for the easy test case, a mesh with 210×100 elements is used. An initial time step equal to 10^{-15} s and a maximal time step equal to 0.1 s have been used.

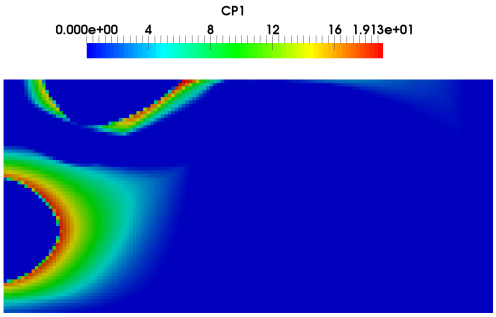

Figure 5: Concentration of component P_1 at $t = 2000$ s for the 2D advective hard test case.

4.2.2. Interaction of CO_2 with minerals

In the context of the geological sequestration of CO_2, several physical and geochemical trapping mechanisms can be combined. Among these different possible mechanisms, geological and solubility trappings are more effective in the short term, but mineral trapping is safer and more economical in the long term. We consider here an example introduced in [15, 31]. This academic example aims to model the desired mechanism by considering the interactions between CO_2 and minerals through a simplified chemical system depicted in Table 1.

The four reactions are in equilibrium and involve 6 aqueous species and 3 minerals (Calcite, mineral A (MinA) and mineral B (MinB)). Calcite and mineral B are carbonates while mineral A is a silicate. The first two reactions allow the transformation of $CO_{2(l)}$ into HCO_3^- and Calcite. These reactions increase the concentration of H^+ and the mineral A is dissolved and releases metal ions Me^{3+}. Finally, these ions Me^{3+} react with HCO_3^- to precipitate the mineral B.

No.	Reactions	K
(1)	$CO_{2(l)} + H_2O \rightleftharpoons HCO_3^- + H^+$	0.1
(2)	$Calcite + H^+ \rightleftharpoons Ca^{2+} + HCO_3^-$	100
(3)	$MinA + 3H^+ \rightleftharpoons Me^{3+} + SiO_{2(l)}$	10
(4)	$MinB + 2\,H^+ \rightleftharpoons Me^{3+} + HCO_3^-$	1.25

Table 1: Chemical reactions.

Table 2 displays some physical parameters for this example. As for the MoMaS hard test case, for each mineral reaction, a solubility product (28) must be respected. For instance for calcite:

$$\frac{c_{Ca^{2+}}\, c_{HCO_3^-}}{c_{H^+}} = 100 \text{ if } c_{Calcite} > 0. \tag{31}$$

Domain	$\Omega =]0, 10[\times]0, 6[$
Darcy velocity	$\vec{q} = (0, 015, 0)^T$
Porosity	$\phi = 0.3$
Longitudinal dispersion	$d_L = 0.3$
Longitudinal dispersion	$d_T = 0.03$
Molecular diffusion	$D_m = 0$

Table 2: Physical parameters.

The initial values are $c_{CO_{2(l)}} = c_{HCO_3^-} = c_{SiO_{2(l)}} = 1$, $c_{H^+} = 0.1$, $c_{Me^{3+}} = 0.01$ and $c_{Ca^{2+}} = 10$ (constant in Ω). For the minerals, $c_{MinA} = 0.2$ for $x \geq 6$, $c_{Calcite} = 0.2$ for $1 < x < 6$ and zero else and $c_{MinB} = 0$. Dirichlet boundary conditions are enforced for the mobile species on the left of the domain with the following values: $c_{CO_{2(l)}} = 3.787$, $c_{H^+} = 0.3124$, $c_{HCO_3^-} = 1.212$, $c_{Me^{3+}} = 0.01$, $c_{SiO_{2(l)}} = 1$ and $c_{Ca^{2+}} = 10$ on $\{0\} \times [1.5, 4.5]$, while the initial values are imposed on the rest of the left border. For the top and bottom border, homogeneous Neumann boundary condition is given while an outflow boundary condition (zero concentration gradient and pure advective flux) is imposed at the outlet. The spatial and time steps are respectively $h = 0.1$ and $\Delta t = 0.1$ as in [15] leading to a mesh composed of 6000 cells. Figures 6–8 visualize the numerical results at $t = 40\ s$, $200\ s$ and $360\ s$. As

expected, dissolved $CO_{2(l)}$ and H^+ ions enters into the domain decreasing the pH. Then calcite and mineral A are dissolved by the front of low pH water stream. Finally, the dissolution of mineral A induces the precipitation of mineral B. These results are in very good agreement with those obtained in [15, 31].

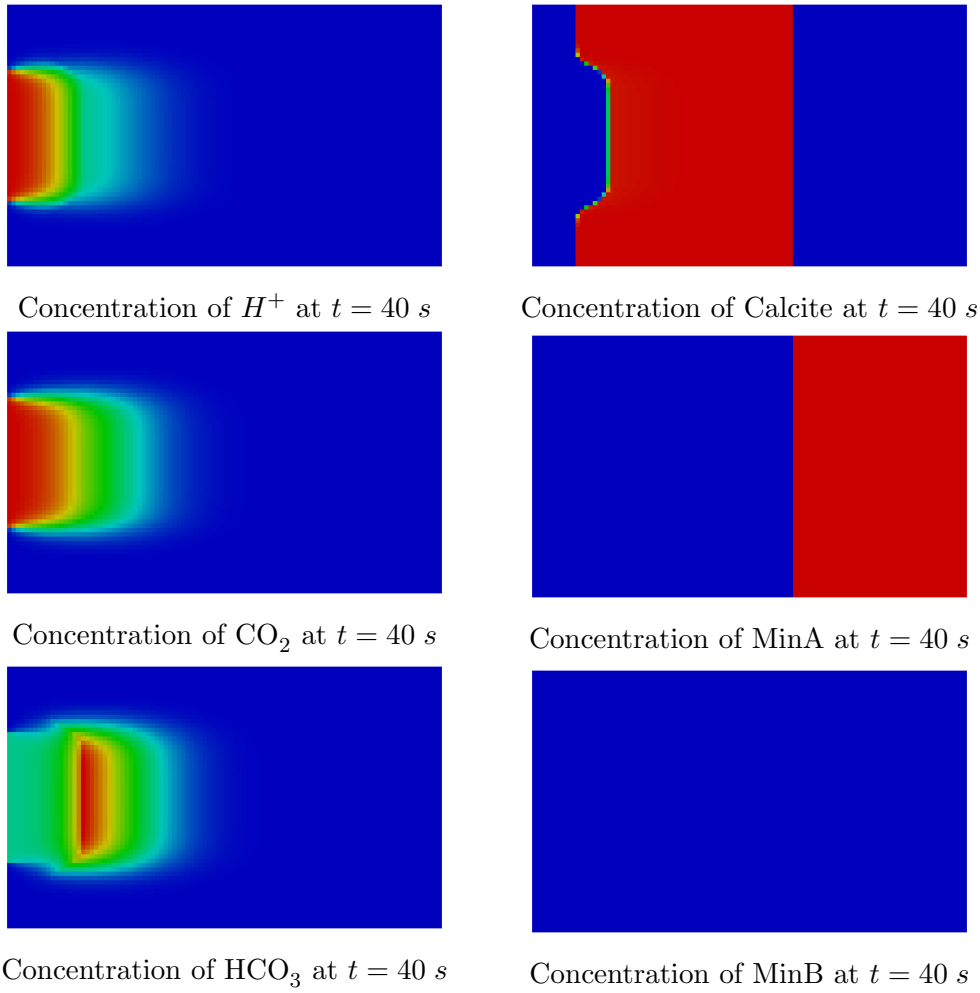

Concentration of H^+ at $t = 40\ s$ | Concentration of Calcite at $t = 40\ s$

Concentration of CO_2 at $t = 40\ s$ | Concentration of MinA at $t = 40\ s$

Concentration of HCO_3 at $t = 40\ s$ | Concentration of MinB at $t = 40\ s$

Figure 6: Profiles of concentrations at $t = 40\ s$.

4.2.3. SHPCO2 test case

This test case was proposed in the framework of the SHPCO2 Project (French acronym for High Performance Simulation of CO_2 Geological Stor-

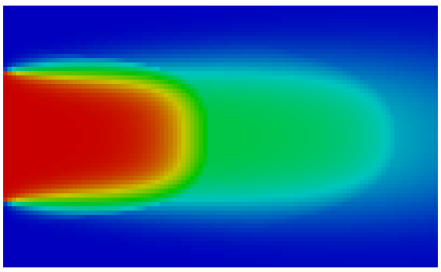

Concentration of H^+ at $t = 200\ s$

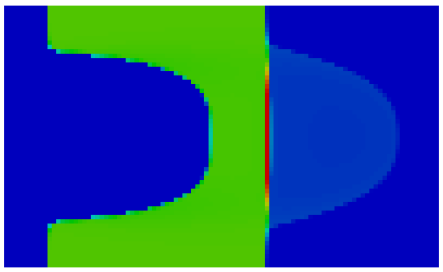

Concentration of Calcite at $t = 200\ s$

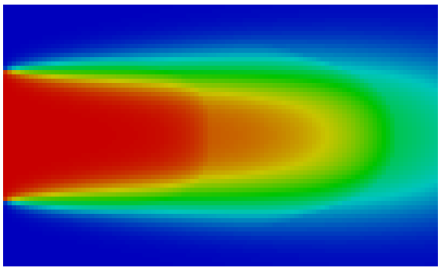

Concentration of CO_2 at $t = 200\ s$

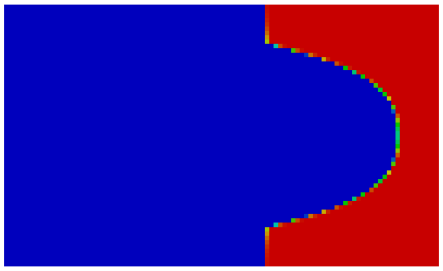

Concentration of MinA at $t = 200\ s$

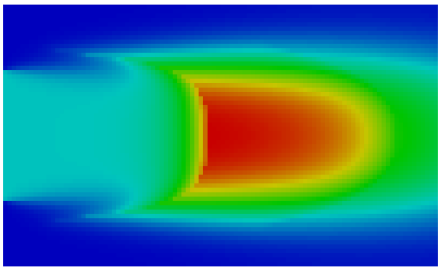

Concentration of HCO_3 at $t = 200\ s$

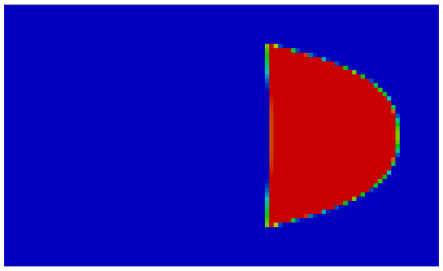

Concentration of MinB at $t = 200\ s$

Figure 7: Profiles of concentrations at $t = 200\ s$.

age). Its detailed description can be found in [25]. The chemical system consists of components involved in 4 reactions displayed in Table 3. The species Cl plays the role of a tracer component. It does not participate in any chemical reaction and its presence has no influence on any physical parameters of the system.

We consider firstly the two-dimensional version of the test. The geometry of the domain is depicted in Figure 9. It is divided into two zones: a "barrier" zone with a low permeability $K_{\text{barrier}} = 10^{-15}\ m^2$ (represented in green in Figure 9) and a "drain" zone (the remaining part) with higher permeability

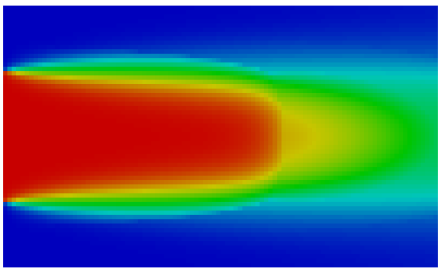

Concentration of H^+ at $t = 360\ s$

Concentration of Calcite at $t = 360\ s$

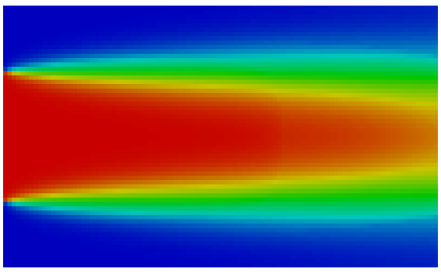

Concentration of CO_2 at $t = 360\ s$

Concentration of MinA at $t = 360\ s$

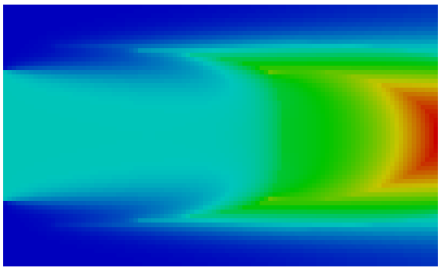

Concentration of HCO_3 at $t = 360\ s$

Concentration of MinB at $t = 360\ s$

Figure 8: Profiles of concentrations at $t = 360\ s$.

$K_{\text{drain}} = 10^{-13}\ m^2$.

In this test, the gas phase is assumed to be immobile and therefore gaseous carbon dioxide $CO_{2(g)}$ is considered as a fixed species. The hypothesis of immobility of gas allows to focus on reactive transport without worrying issues of multiphase flow. Consequently, the problem is modelled by a single phase multicomponent flow with reactive transport.

Initially, in the orange bubble of Figure 9 gaseous carbon dioxide $CO_{2(g)}$ is present while in the remaining zone, concentration of $CO_{2(g)}$ is equal to zero. For the flow, Dirichlet boundary conditions for the pressure are enforced at

No.	Reactions
(1)	$OH^- + H^+ \rightleftharpoons H_2O$
(2)	$CO_{2(g)} \rightleftharpoons CO_{2(l)}$
(3)	$HCO_3^- + H^+ \rightleftharpoons CO_{2(l)} + H_2O$
(4)	$Calcite + H^+ \rightleftharpoons Ca^{2+} + HCO_3^-$

Table 3: Chemical reactions for the SHPCO2 test case.

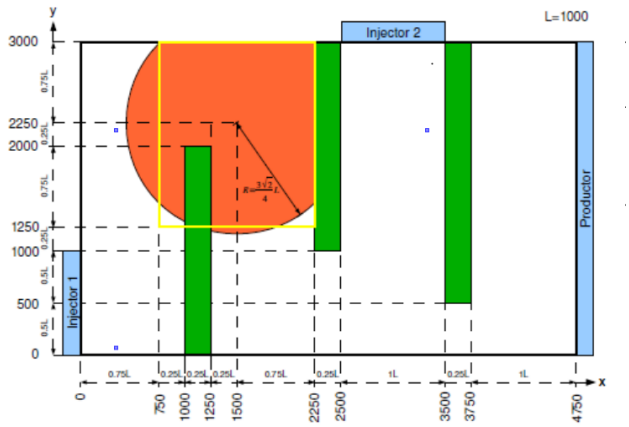

Figure 9: Two-dimensional geometry of domain for the SHPCO2 test case.

the boundary surfaces Injector1, Injector2 and Productor while at the rest of the boundary of the domain, homogeneous Neumann condition are imposed. Concerning the transport, a pure advective flux on the boundary surfaces Injector1, Injector2 and Productor is imposed. On the rest of the boundary of the domain, we consider homogeneous Neumann conditions. Physical parameters and initial concentrations can be found in [7]. The period of simulation is equal to 4500 years. Several two-dimensional meshes have been used. An adaptive time step strategy is used with a maximal time step equal to 10 years.

Figure 10 represents the evolution of the concentration of $CO_{2(g)}$ and $CO_{2(aq)}$ at $t = 400$ years and $t = 1600$ years with a mesh composed of 233472 elements. Due to the hypothesis of the immobility of the gas phase, the position of zone with $CO_{2(g)}$ does not change with time but its size is significantly reduced. This is explained by the fact that $CO_{2(g)}$ dissolves in

liquid phase and is transported by flow outside the initial gaseous zone.

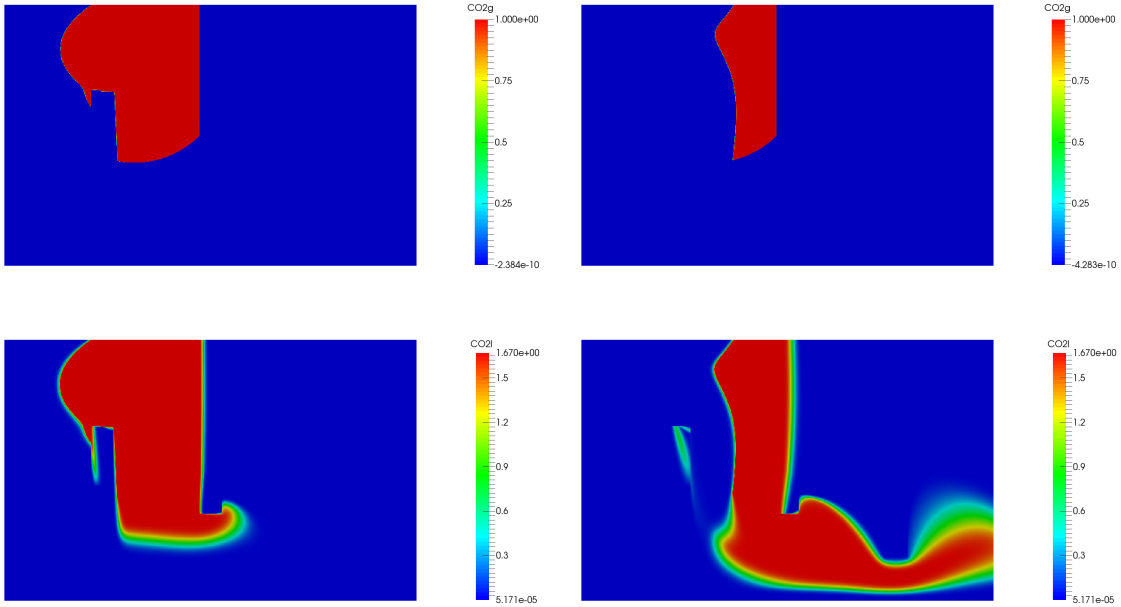

Figure 10: Evolution of the concentrations of $CO_{2(g)}$ and $CO_{2(aq)}$. Left: 400 years. Right: 1200 years.

Convergence analysis. Several meshes (see Table 4) have been considered for this test case.

Mesh	XS	S	M	L	XL
h	125	62.5	31.25	15.625	7.8125
Nx	38	76	152	304	608
Ny	24	48	96	192	384
NCell	912	3648	14592	58368	233472

Table 4: Parameters for 2D meshes.

The finest mesh composed of 233472 elements is assumed to provide a reference solution $c^{ref}_{H^+}$. Figure 11 displays on a logarithmic-scale the L^2-norm $||c^{ref}_{H^+} - c^h_{H^+}||$ for several values of h. We can observe a first order convergence.

Figure 12 depicts the concentrations c_{H^+} for the difference meshes on the line $y = 600$. As expected, the concentration c_{H^+} converge toward the reference solution when the space step h decreases.

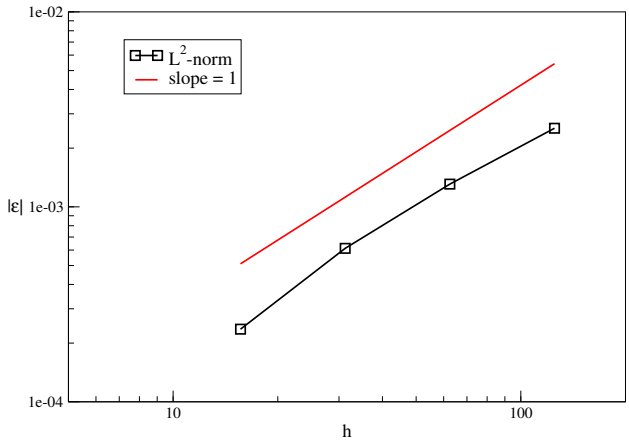

Figure 11: Logarithmic plot for $||c^{ref}_{\mathrm{H}^+} - c^{h}_{\mathrm{H}^+}||$ as a function of the space step h.

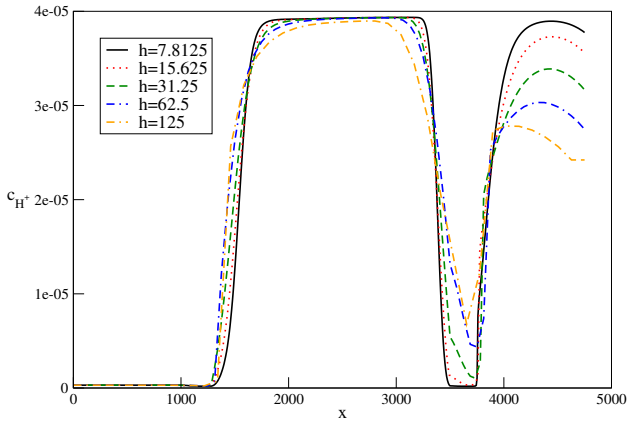

Figure 12: Comparison of the concentration of H^+ obtained with several meshes.

4.2.4. Comparison between DSA ad SIA

This subsection aims to compare DSA and SIA in the same numerical environment for the example presented above. Both approaches adopt an adaptive time-stepping. In the DSA, the control of the time-step is based on

the number of iterations required by the Newton method to achieve convergence while in the SIA, it is based on the number of iterations required in the iterative algorithm to reach the tolerance ϵ_{SIA}. In the sequel, tolerances for the Newton method and iterative algorithm are respectively $\epsilon_{Newton} = 10^{-8}$ and $\epsilon_{SIA} = 10^{-5}$.

Figure 13 compares the concentration of $CO_{2(aq)}$ obtained with DSA and SIA on the line $y = 600$ with two meshes composed of 14592 and 58368 cells at $t = 1600$ years. We can observe that the results are in great accordance.

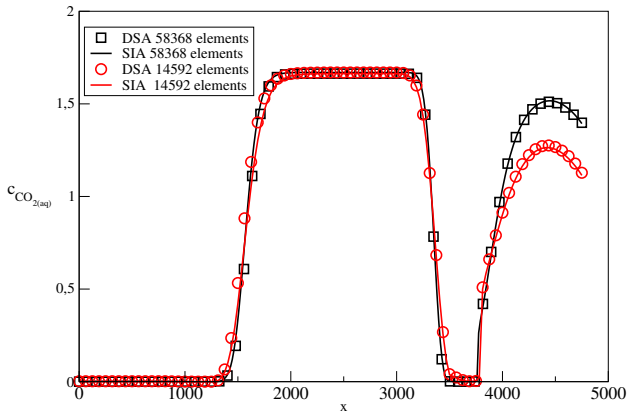

Figure 13: Comparison of the concentration of $CO_{2(aq)}$ obtained with DSA and SIA.

Table 5 displays the CPU time required and the number of time steps for the DSA and the SIA to reach 1200 years on several meshes. We can see that for this example, DSA is faster than SIA when fine meshes are used. Figure 14 a) represents the time steps used by the DSA and SIA during the computations for the two finest meshes. We have to specify that a maximum time step equal to 10 years was enforced. We can remark that the implicit approach allows to use larger time steps than the sequential approach. This is emphasized by Figure 14 b) that depicts the number of iterations required by the Newton method to achieve ϵ_{Newton} in the DSA and the number of iterations required in the SIA to reach the tolerance ϵ_{SIA}. The results are given for the mesh composed of 58368 elements. We can see that the SIA requires more iterations than the DSA and therefore, the time step can not increase as quickly as for the DSA and never reaches the maximum value equal to 10 years.

	DSA		SIA	
Mesh	CPU time(s)	Number of time steps	CPU time(s)	Number of time steps
XS	1118	567	741	572
S	2272	578	2288	572
M	8612	578	11439	575
L	27143	579	72813	626

Table 5: CPU time (s) and number of time steps for DSA and SIA.

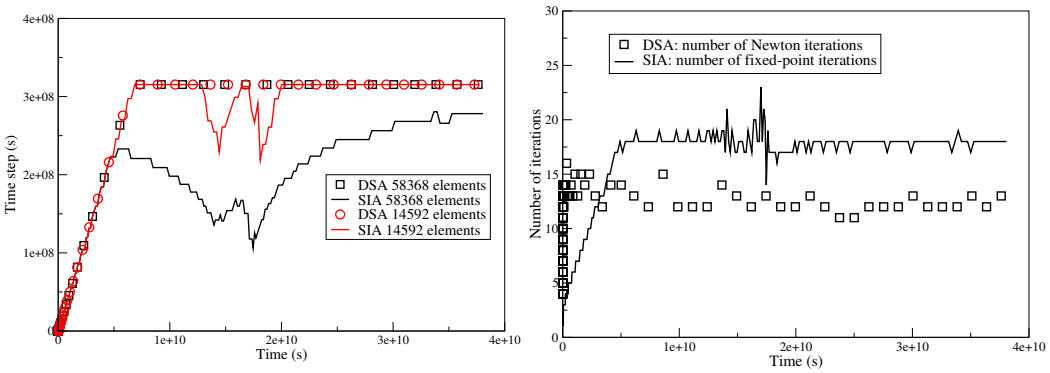

a) Time step versus time.

b) Number of iteratons versus time.

Figure 14: Comparison between DSA ad SIA.

4.2.5. Three-dimensional simulation

Finally, to check the robustness of our approach and its ability to deal with real three dimensional configurations, we have performed the three-dimensional version of the test. The geometry is represented in Figure 15.

Figure 16 represents several quantities after 1500 years of simulation on a mesh composed of 912000 elements. The computation has been performed with 256 processors. As for the two-dimensional case, the initial bubble of gaseous $CO_{2(g)}$ is dissolved and transported in liquid phase. The concentrations of H^+ and $CO_{2(aq)}$ are very correlated since high concentrations of $CO_{2(aq)}$ acidify the medium.

Parallel performance.

Parallelization in the DuMu^X is carried out using the DUNE [12, 13] parallel library package. DUNE gives arbitrary data decomposition in a generic way and the employed assembly operator and linear solvers are designed corre-

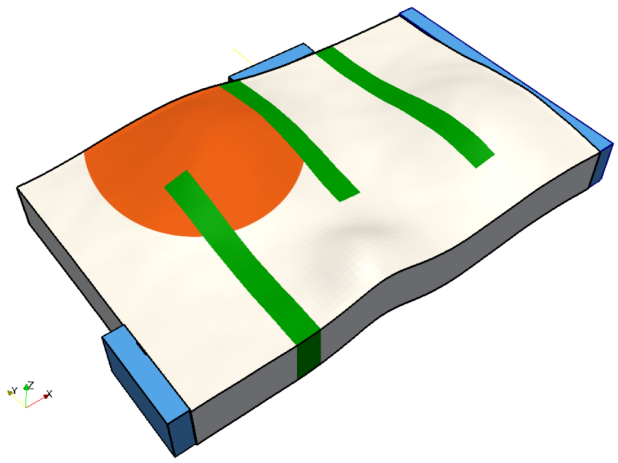

Figure 15: Three-dimensional geometry of domain for the SHPCO2 test case.

spondingly. Parallel computations on a hierarchical grid follow the "single program multiple data" (SPMD) programming paradigm based on a suitable decomposition of the grid entities. Tasks are divided and run simultaneously on several processors with different input. Processors execute their own program and communicate with each other using the Message Passing Interface (MPI).

Parallel computations up to 512 processors have been performed on several grids. The parallel efficiency of our strategy is illustrated by solving 100 time steps. The code ran on a Bull cluster named OCCIGEN with Intel "Haswell" 12-Core E5-2690 V3 processors. In parallel computing, two types of scalability are defined. The first is the strong scaling, which represents the relation between the computation time and the number of processors for a fixed total problem size. The second is the weak scaling, for which the load per processor is fixed.

Strong scaling

Figure 17 a) displays on a logarithmic scale, CPU time as a function of the number of processors for 2 size problems of 228000 and 912000 elements corresponding to approximately 1.6×10^6 and 6.4×10^6 unknowns. The dashed lines represent an ideal behaviour.

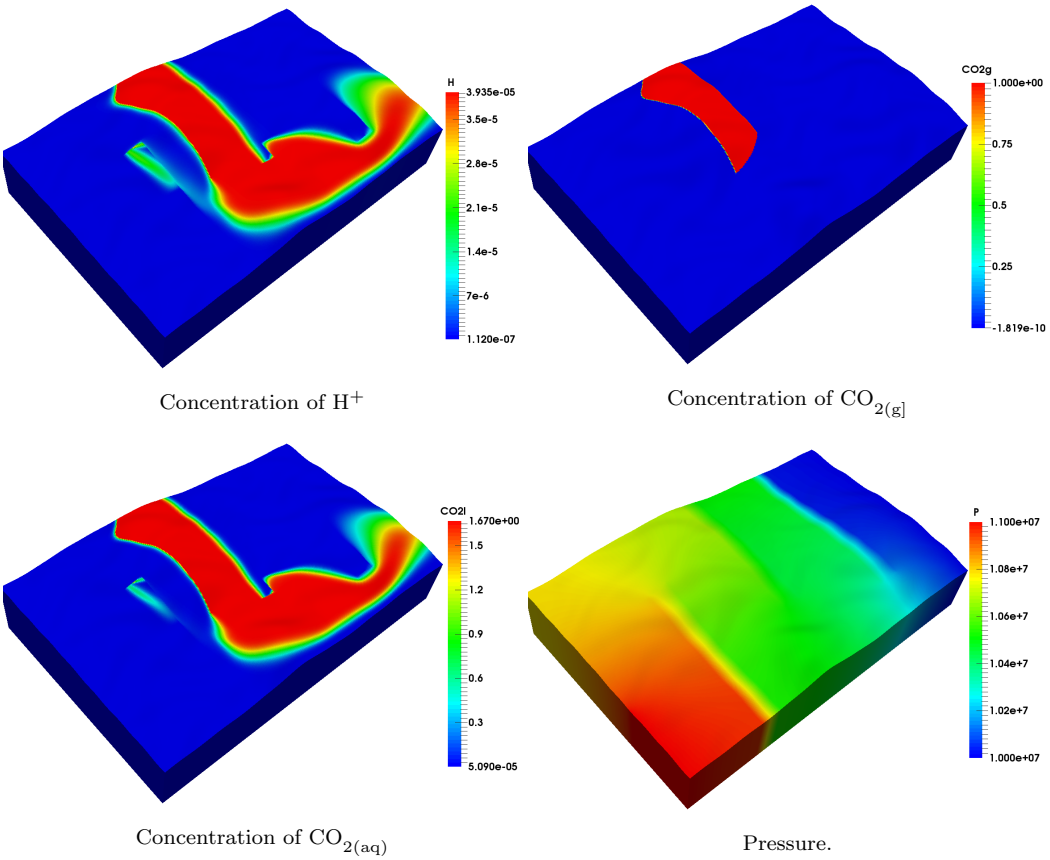

Concentration of H^+

Concentration of $CO_{2(g]}$

Concentration of $CO_{2(aq)}$

Pressure.

Figure 16: Profiles of concentrations and pressure at $t = 1500$ years.

Strong efficiency is given by:

$$SE(N) = \frac{\text{CPU time on } p \text{ processors } \times p}{\text{CPU time on } N \text{ processors } \times N}, \tag{32}$$

here p denotes the number of processors used for the reference time (not always equal to one for heavy computations). For both calculations, we took $p = 8$. It points out an optimal use of the parallel resources. Efficiency equal to one indicates that communications and synchronizations between processors are negligible.

Figure 17 b) represents the strong scaling versus the number of processors. A high efficiency (greater than 0.85) is observed up to 256 processors for the computations involving 912000 cells. For the simulation with 228000 cells,

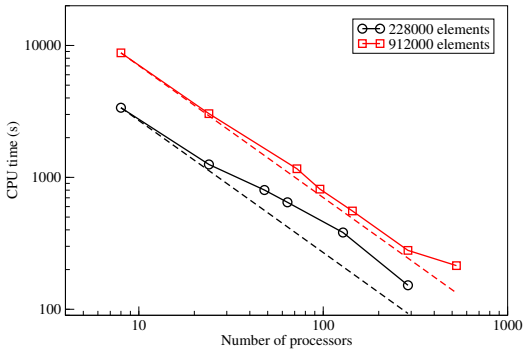

a) CPU time versus the number of processors

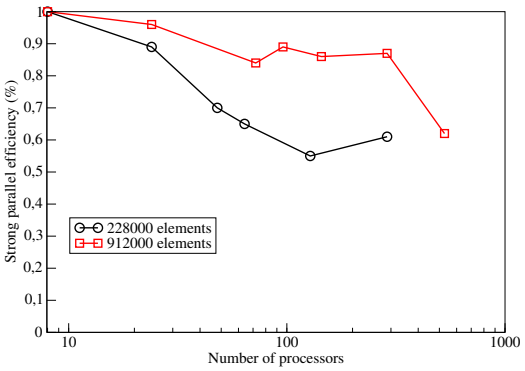

b) Strong parallel efficiency

Figure 17: CPU time and strong parallel efficiency as a function of the number of processors.

the efficiency is good up to 64 processors. The loss of efficiency is mainly due to the increase of the communications between processors in comparison with the load of each processor.

Weak scaling

Figure 18 a) displays CPU time as a function of the number of processors, with 9120 and 18240 elements per processor. Weak efficiency is given by:

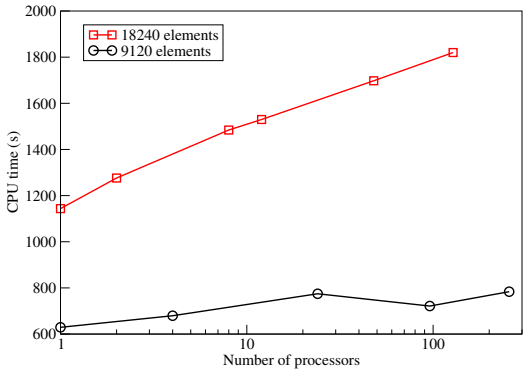

a) CPU time versus the number of processors

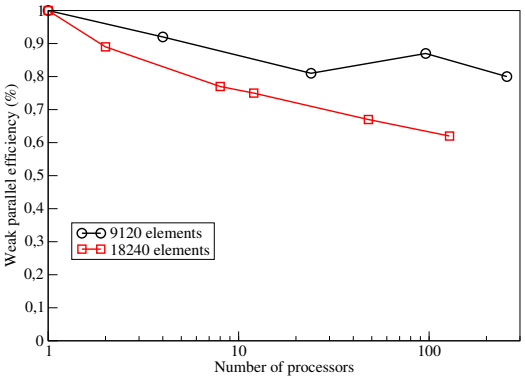

b) Weak parallel efficiency

Figure 18: CPU time and weak parallel efficiency as a function of the number of processors.

$$WE(N) = \frac{\text{CPU time on } p \text{ processors}}{\text{CPU time on } N \text{ processors}}, \tag{33}$$

where p still denotes the number of processors used for the reference time. Here, $p = 1$ for the two scenarios. Efficiency equal to one indicates an optimal behaviour for the algorithm and the computer architecture. Indeed, CPU times remains constant, equal to the reference time, while the total size of the problem increases with the number of processors. Usually, this property is hardly verified and curves with plateaus can be observed. This phenomenon is illustrated in Figure 18 b).

5. Conclusion

In this work we have considered a GIA for the simulation of single phase multicomponent flows with reactive transport in porous media. More precisely, a fully implicit finite volume scheme of a DSA has been developed and implemented in the framework of the parallel free and open-source platform DuMu^X. Several test cases have been performed and gave numerical results close to those obtained in the literature. Some 3D parallel computations have been done with good strong and weak parallel efficiencies. Furthermore, this paper features a rigorous numerical investigation to give a comparative evaluation of the DSA and the SIA for single phase flow with reactive transport in porous media. As mentioned before, throughout the past decades, many numerical codes were developed to solve reactive transport problems in porous media. However, when it comes to mathematical and numerical analysis of the model equations, the literature becomes scarcer. This study was intended as a first step to the numerical analysis of two-phase multicomponent flow with reactive transport in heterogeneous reservoirs. These more complicated cases appear in many applications. Further work in these important issues are in progress.

Acknowledgments

This research has been supported by Institut Carnot ISIFoR (Institute for the sustainable engineering of fossil resources). This support is gratefully acknowledged. We also thank the DuMu^X and DUNE teams for their help during the development of our reactive transport module and the CINES (National Computing Center for Higher Education) to give us access to their computing resources facility. This work was granted access to the HPC resources of CINES under the allocations 2017-A0010610019, 2017-A0020610019 and 2018-A0040610019 made by GENCI. The authors gratefully thank the anonymous referees for their insight comments and suggestions.

References

[1] DuMu^X, DUNE for Multi-{Phase, Component, Scale, Physics, ...} flow and transport in porous media, http://www.dumux.org, Last accessed February 1, 2018.

[2] DUNE, the Distributed and Unified Numerics Environment, http://www.dune-project.org, Last accessed February 1, 2018.

[3] GSL multidimensional root-finding, http://www.gnu.org/software/gsl/, Last accessed February 1, 2018.

[4] N. Ahmad, A. Wörman, A. Bottacin-Busolin, X. Sanchez-Vila, Reactive transport modeling of leaking CO_2-saturated brine along a fractured pathway, International Journal of Greenhouse Gas Control 42 (2015) 672–689.

[5] N. Ahmad, A. Wörman, X. Sanchez-Vila, J. Jarsjö, A. Bottacin-Busolin, H. Hellevang, Injection of CO_2 saturated brine in geological reservoir: A way to enhanced storage safety, International Journal of Greenhouse Gas Control 54 (2016) 129–144.

[6] E. Ahusborde, B. Amaziane, M. El Ossmani, Finite volume scheme for coupling twophase flow with reactive transport in porous media, Finite Volumes for Complex Applications VIII-Hyperbolic, Elliptic and Parabolic Problems, Springer Proceedings in Mathematics and Statistics 200 (2017) 407–415.

[7] E. Ahusborde, M. El Ossmani, A sequential approach for numerical simulation of two-phase multicomponent flow with reactive transport in porous media, Mathematics and Computers in Simulation 137 (2017) 71–89.

[8] E. Ahusborde, M. Kern, V. Vostrikov, Numerical simulation of two-phase multicomponent flow with reactive transport in porous media: application to geological sequestration of CO_2, ESAIM: Proceedings and Surveys 50 (2015) 21–39.

[9] R. Al-Khoury, J. Bundschuh, Computational Models for CO_2 Geosequestration & Compressed Air Energy Storage, Sustainable Energy Developments, CRC Press, 2014.

[10] L. Amir, M. Kern, A global method for coupling transport with chemistry in heterogeneous porous media, Computational Geosciences 14 (2010) 465–481.

[11] D.A. Barry, C.T. Miller, P.J. Culligan-Hensley, Temporal discretisation errors in non-iterative split-operator approaches to solving chemical reaction/groundwater transport models, Journal of Contaminant Hydrology 22 (1996) 1–17.

[12] P. Bastian, M. Blatt, A. Dedner, C. Engwer, R. Klöfkorn, R. Kornhuber, M. Ohlberger, O. Sander, A generic grid interface for parallel and adaptive scientific computing. part ii: Implementation and tests in dune, Computing 82 (2008) 121–138.

[13] P. Bastian, M. Blatt, A. Dedner, C. Engwer, R. Klöfkorn, M. Ohlberger, O. Sander, A generic grid interface for parallel and adaptive scientific computing. part i: Abstract framework, Computing 82 (2008) 103–119.

[14] C. Bethke, Geochemical and biogeochemical reaction modeling: Second edition, Cambridge University Press, 2007.

[15] H. Buchholzer, C. Kanzow, P. Knabner, S. Kräutle, The semismooth newton method for the solution of reactive transport problems including mineral precipitation-dissolution reactions, Comput. Optim. Appl. 50 (2011) 193–221.

[16] J. Carrayrou, Looking for some reference solutions for the reactive transport benchmark of MoMaS with SPECY, Computational Geosciences 14 (2010) 393–403.

[17] J. Carrayrou, J. Hoffmann, P. Knabner, S. Kräutle, C. de Dieuleveult, J. Erhel, J. Van der Lee, V. Lagneau, K.U. Mayer, K.T.B. MacQuarrie, Comparison of numerical methods for simulating strongly nonlinear and heterogeneous reactive transport problems–the MoMaS benchmark case, Computational Geosciences 14 (2010) 483–502.

[18] J. Carrayrou, M. Kern, P. Knabner, Reactive transport benchmark of MoMaS, Computational Geosciences 14 (2010) 385–392.

[19] I.P. on Climate Change (IPCC), IPCC special report on carbon dioxide capture and storage, in: B. Metz, O. Davidson,

H.C. de Coninck, M. Loos, L.A. Meyer (Eds.), IPCC Special Report on Carbon Dioxide Capture and Storage, Cambridge University Press, 2005. URL: http://www.ipcc.ch/pdf/special-reports/srccs/srccs_wholereport.pdf, prepared by Working Group III of the Intergovernmental Panel on Climate Change.

[20] C. de Dieuleveult, J. Erhel, A global approach to reactive transport: Application to the MoMaS benchmark, Computational Geosciences 14 (2010) 451–464.

[21] J. Erhel, S. Sabit, Analysis of a global reactive transport model and results for the MoMaS benchmark, Mathematics and Computers in Simulation 137 (2017) 286–298.

[22] Y. Fan, L.J. Durlofsky, H.A. Tchelepi, A fully-coupled flow-reactive-transport formulation based on element conservation, with application to CO_2 storage simulations, Advances in Water Resources 42 (2012) 47–61.

[23] A. Fischer, A special Newton-type optimization method, Optimization (1992) 269–284.

[24] B. Flemisch, M. Darcis, K. Erbertseder, B. Faigle, A. Lauser, K. Mosthaf, S. Muthing, P. Nuske, A. Tatomir, M. Wolf, R. Helmig, DuMu^X: DUNE for Multi-{Phase, Component, Scale, Physics, ...} flow and transport in porous media, Advances in Water Resources 34(9) (2011) 1102–1112.

[25] F. Haeberlein, Time Space Domain Decomposition Methods for Reactive Transport – Application to CO_2 Geological Storage, Ph.D. thesis, Université Paris-Nord - Paris XIII, 2011.

[26] R. Helmig, Multiphase flow and transport processes in the subsurface: a contribution to the modeling of hydrosystems, Springer, 1997.

[27] J. Hoffman, Reactive Transport and Mineral Dissolution/Precipitation in Porous Media: Efficient Solution Algorithms, Benchmark Computations and Existence of Global Solutions, Ph.D. thesis, University of Erlangen, 2010.

[28] J. Hoffmann, S. Kräutle, P. Knabner, A parallel global-implicit 2-D solver for reactive transport problems in porous media based on a reduction scheme and its application to the MoMaS benchmark problem, Computational Geosciences 14 (2010) 421–433.

[29] J. Hoffmann, S. Kräutle, P. Knabner, A general reduction scheme for reactive transport in porous media, Computational Geosciences 14 (2012) 1081–1099.

[30] X. Jiang, A review of physical modelling and numerical simulation of long-term geological storage of CO_2, Applied Energy 88 (2011) 3557–3566.

[31] S. Kräutle, General multi-species reactive transport problems in porous media: efficient numerical approaches and existence of global solutions, Habilitation Thesis, University of Erlangen, Germany, 2008.

[32] S. Kräutle, P. Knabner, A new numerical reduction scheme for fully coupled multicomponent transport-reaction problems in porous media, Water Resources Research 41 (2005) 1–17.

[33] S. Kräutle, P. Knabner, A reduction scheme for coupled multicomponent transport-reaction problems in porous media: Generalization to problems with heterogeneous equilibrium reactions, Water Resources Research 43 (2007).

[34] V. Lagneau, J. van der Lee, HYTEC results of the MoMaS reactive transport benchmark, Computational Geosciences 14 (2010) 435–449.

[35] V. Lagneau, A. Pipart, H. Catalette, Reactive transport modelling of CO_2 sequestration in deep saline aquifers, Oil & Gas Science and Technology 60 (2005) 231–247.

[36] A. Lauser, C. Hager, R. Helmig, B. Wohlmuth, A new approach for phase transitions in miscible multi-phase flow in porous media, Advances in Water Resources 34 (2011) 957–966.

[37] P.C. Lichtner, Continuum model for simultaneous chemical reactions and mass transport in hydrothermal systems, Geochimica et Cosmochimica Acta 49 (1985) 779–800.

[38] K.U. Mayer, K.T.B. MacQuarrie, Solution of the MoMaS reactive transport benchmark with MIN3P-model formulation and simulation results, Computational Geosciences 14 (2010) 405–419.

[39] S. Molins, J. Carrera, C. Ayora, M.W. Saaltink, A formulation for decoupling components in reactive transport problems, Water Resources Research 40 (2004) 1–13.

[40] F.M. Morel, J.G. Hering, Principles and applications of aquatic chemistry, Wiley, New York, 1993.

[41] J.P. Nicot, S.A. Hosseini, S.V. Solano, Are single-phase flow numerical models sufficient to estimate pressure distribution in CO_2 sequestration projects?, Energy Procedia 4 (2011) 3919–3926.

[42] A. Niemi, J. Bear, J. Bensabat, Geological Storage of CO_2 in Deep Saline Formations, Springer, 2017.

[43] M. Pool, J. Carrera, V. Vilarrasa, O. Silva, C. Ayora, Dynamics and design of systems for geological storage of dissolved CO_2, Advances in Water Resources 62 (2013) 533–542.

[44] C.I. Steefel, K.T.B. MacQuarrie, Approaches to modeling of reactive transport in porous media, Reviews in Mineralogy 34 (1996) 82–129.

[45] A.J. Valocchi, M. Malmstead, Accuracy of operator splitting for advection-dispersion-reaction problems, Water Resources Research 28 (1992) 1471–1476.

[46] G.T. Yeh., V.S. Tripathi, A model for simulating transport of reactive multispecies components: Model development and demonstration, Water Resources Research 27 (1991) 3075–3094.